International Journal of Thermophysics, Vol. 16, No. 5, 1995

Structure and Dynamics of Water-in-Oil Microemulsions Near the Critical and Percolation Points[1]

C. Y. Ku,[2] S. H. Chen,[2,3] J. Rouch,[4] and P. Tartaglia[5]

The three-component ionic microemulsion system consisting of AOT/water/decane shows an interesting phase behavior in the vicinity of room temperature. The phase diagram in the temperature–volume fraction (of the dispersed phase) plane exhibits a lower consolute critical point at about 40°C and 8% volume fraction. A percolation line, starting from the vicinity of the critical point, cuts across the plane, extending to the high-volume fraction side at progressively lower temperatures. This phase behavior can be understood in terms of a system of polydispersed spherical water droplets, each coated by a monolayer of AOT, dispersed in a continuum of oil. These droplets interact with each other via a hard-core plus a short-range attractive interaction, the strength of which increases with temperature. We show that Baxter's sticky-sphere model can account quantitatively for the phase behavior, including the percolation line, provided that the stickiness parameter is a suitable function of temperature. We use the structure factors measured by small-angle neutron scattering below the critical temperature to determine this functional dependence. We also investigate the dynamics of droplets, below and approaching the critical and percolation points, by dynamic light scattering. Both the Q dependence of the first cumulant and the time evolution of the droplet density correlation function can be quantitatively calculated by assuming the existence of polydispersed fractal clusters formed by the microemulsion droplets due to attraction.

KEY WORDS: microemulsion; percolation; sticky-sphere model.

[1] Invited paper presented at the Twelfth Symposium on Thermophysical Properties, June 19–24, 1994, Boulder, Colorado, USA.

[2] Department of Nuclear Engineering, Massachusetts Institute of Technology, Cambridge, Massachusetts 02139, USA.

[3] To whom correspondence should be addressed.

[4] CPMOH, Universite Bordeaux I, 351 Cours de la Liberation, 33405 Talence, France.

[5] Dipartimento de Fisica, Universita di Roma "La Sapienza," P. le Aldo Moro 2, I-00185 Rome, Italy.

0195-928X/95/0900-1119$07.50/0

1. INTRODUCTION

The three-component ionic microemulsion system made of anionic surfactant, sodium di-2-ethylhexylsulfosuccinate (AOT), water, and decane is rather unusual in terms of its phase behavior. At a constant temperature, a typical symmetric ternary microemulsion system, having equal volume fractions of water and oil, shows the well-known 2–3–1 phase progression, as the surfactant concentration is increased from 0 to more than 8%. When the surfactant concentration is very low, the molecules are dispersed in water and oil just as monomers. The system is naturally phase-separated into two phases, with an oil-rich phase on the top and a water-rich phase in the bottom, because of high interfacial tension between water and oil. There is no organized structure in the two phases. At a temperature at which the surfactant has balanced affinities toward water and oil, a three-phase coexistence, with a middle-phase microemulsion in coexistence with an oil-rich phase on the top and a water-rich phase in the bottom, is to be expected at relatively higher surfactant concentrations simply because of a finite solubilization power of the surfactant for water and oil. The middle-phase microemulsion is an interesting liquid because there is an organized microstructure in it. The microemulsion shows ultralow interfacial tensions between itself and the water and oil-rich phases. The microstructure of the middle-phase microemulsion is often described as being "biscontinuous" in both water and oil. With further increase in the surfactant concentration, a "minimum" concentration will be reached whereby all the excess water and oil are solubilized into a single-phase microemulsion. This minimum concentration is usually between 5 and 8% for a good microemulsion system. The value of the minimum concentration is a measure of amphiphilicity of the surfactant molecules at that temperature, being lower for higher amphiphilicity. In the vicinity of this minimum surfactant concentration, the microstructure of the one-phase microemulsion is also disordered bicontinuous [1]. As the surfactant concentration further increases, the one-phase microemulsion transforms into a lamellar structure, which may be called ordered bicontinuous, and then to some other three-dimensional ordered structures. This disorder-to-order transition occurs usually around 15% of the surfactant concentration.

The AOT/water/decane system, on the other hand, does not follow this usual pattern of phase behavior. Around room temperature the surfactant film, consisting of AOT molecules, possesses a spontaneous curvature toward water due to hydrophilicity–lipophylicity imbalance of AOT molecules in this temperature range. Thus one finds in the ternary phase diagram a large one-phase region, called the L_2 phase, extending from the decane corner into the middle of the phase triangle. In the L_2 phase, even

with equal volume fractions of water and oil, the microemulsion, instead of being bicontinuous, consists of water droplets, coated by a monolayer of AOT, dispersed in decane. With this microstructure, the microemulsion is nearly an insulator because the water droplets are separated from each other. Our previous SANS experiments verified that the average radius $\langle R \rangle$ of the water droplets is determined essentially by the molar ratio of water to AOT, called W, in the system. An approximate empirical relationship between the radius (Å) and W is $\langle R \rangle = (3/2)\, W$. Thus, for $W = 40$, the average water droplet radius is about 60 Å [2]. This water-in-oil droplet structure is maintained even if the volume fractions of water and oil are equal [3], provided the temperature is below 25°C. This case is in sharp contrast to the usual situation that, for equal water and oil volume fractions, the microstructure of one-phase microemulsions was generally found to be bicontinuous [4, 5]. Even for the AOT/water/decane system, when a small amount of salt (NaCl) is added, the common 2–3–1 phase progression is obtained at around the hydrophile–lipophile balance temperature of 40°C [1] and a SANS experiment in the one-phase channel at this temperature conclusively showed that the microstructure is bicontinuous [6].

This persistent droplet structure in the ternary AOT/water/decane system can, however, be used to realize an interesting coexistence of a critical phenomenon at low volume fraction and high temperature and a percolation phenomenon at lower temperatures but at all volume fractions. In fact, this is a rare situation in which one has, in a real system, the realization of both the critical and the percolation points at the same volume fraction.

Figure 1 shows an experimental (open and filled circles) and theoretical (lines) T–ϕ phase diagram of AOT/H_2O/decane system when the water-to-AOT molar ratio $W = 40.8$. Substitution of H_2O by D_2O will merely shift all the phase boundaries up by about 2°. ϕ denotes the volume fraction of the dispersed phase, in this case AOT plus water. In the diagram, one sees a one-phase (L_2) region below 40°C. In the interval of ϕ between 0 and 0.4, there is a cloud point curve separating the one-phase droplet microemulsions from the two-phase droplet microemulsions. The previous SANS experiment established that the average droplet sizes and their size distributions are, within the experimental error, identical in the one-phase and two-phase regions [2]. The critical volume fraction is approximately 0.1 and the critical temperature is 40°C [7] in H_2O. Above the volume fraction of 0.4 there is a phase boundary between the L_2 and a lamellar phase where the microstructure is ordered and bicontinuous in water and decane (not shown in Fig. 1).

The novelty of this phase diagram is, however, the existence of a percolation line, extending from the left of the critical point all the way to

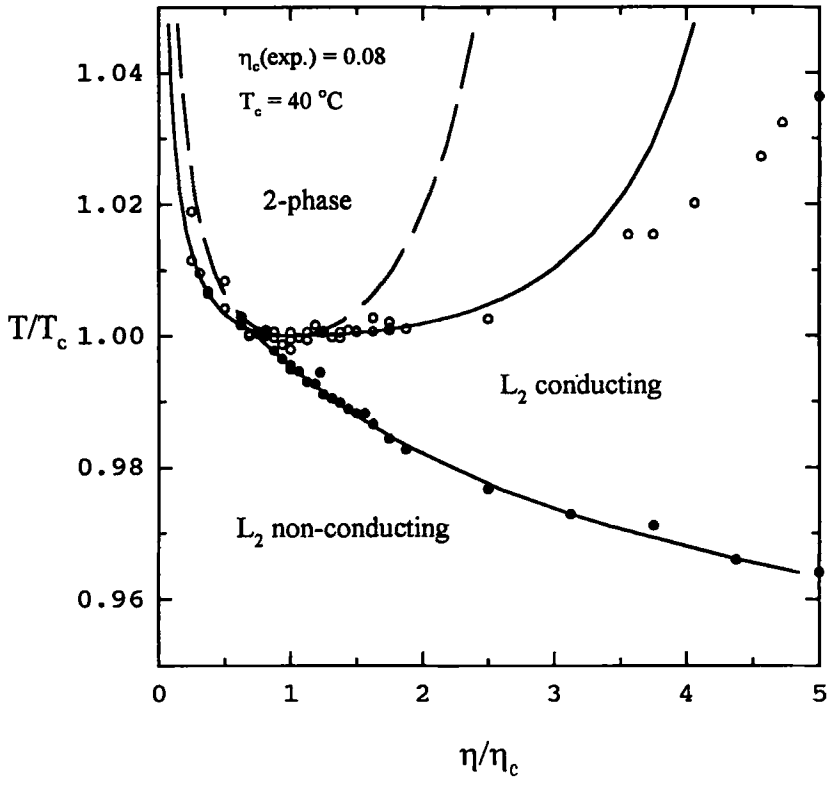

Fig. 1. Projection of the phase prism of the AOT/H_2O/decane system, at $W = 40.8$ and ambient pressure, on the temperature–volume fraction plane. Open circles indicate the phase boundary, and filled circles the percolation locus [8]. The corresponding theoretical coexistence and spinodal curves were calculated based on Baxter's model after the transformation of Eq. (2), with $\alpha = 11$ and $\gamma = 0.94$ (see text). The percolation locus was fitted with Baxter's model by means of the method described in the legend to Fig. 4.

higher volume fractions, gradually decreasing in temperature to about 23°C at $\phi = 0.7$. Below the percolation line the microemulsion is nonconducting, but above the percolation line it becomes conducting. In crossing the line, the conductivity increases by over five orders of magnitude [8]. The asymptotic behavior of conductivity near the threshold, at a given ϕ, can be expressed as power laws in $|T - T_p|$. The divergent indices are $s' = -1.2 \pm 0.1$ coming up from below T_p, and $t = 1.9 \pm 0.1$ going down from above T_p. The exponents are the same when T is fixed but ϕ is varied [8]. The exponent s', determined from conductivities below the threshold, agrees with the value of the index proposed in the so-called dynamic (or

stirred) percolation theory [9, 10], which is distinct from the standard static percolation exponent $s = -0.73$ [11]. On the other hand, the exponent t deduced from data above the threshold agrees with the static or geometric percolation theory [11]. In the theory of dynamic percolation, the conduction of electricity is conjectured to be mediated by charge carriers (presumably the sodium counterions from the AOT molecules) which migrate rapidly among microemulsion droplets forming transient fractal clusters, due to a short-range attractive interaction between the droplets. The percolation threshold is defined theoretically to be a point where the average cluster size becomes infinite, namely, when at least one cluster spans the entire sample. Note that, for this definition, a finite conduction can occur already below the threshold because even there an infinite cluster can exist.

We have thus experimental evidence that the percolation in AOT/water/decane system in the L_2 phase is associated with a clustering phenomenon. The phase diagram that we depict in Fig. 1 should therefore be obtainable from the standard liquid theory with an appropriate definition of the percolation. We outline one such theory in the next section.

2. BAXTER'S STICKY-SPHERE MODEL AND THE ASSOCIATED PHASE DIAGRAM

A reasonable model for a microemulsion in L_2 phase is a collection of spherical colloidal particles of average radius $\langle R \rangle$ interacting among one another via a short-range temperature-dependent attractive pair-potential. This pair-potential can, for example, be a square-well potential with a hard-core diameter of $a - \Delta$, plus an attractive tail of depth $-\varepsilon$ and width Δ. The liquid theory with a square-well potential in general cannot be solved in an analytical form except for a limiting case in which ε tends to infinity and Δ to zero in such a way that the contribution to the second virial coefficient exists. This limiting potential is called Baxter's sticky-sphere potential. By defining a as the outer diameter and σ the inner diameter of the attractive well, it is understood that the limit $\sigma \to a$ is to be taken in the calculation. From our discussion above, it is obvious that $a - \Delta$ is approximately $2\langle R \rangle$. There is a single dimensionless parameter $1/\tau$ in the potential function called the stickiness parameter. The sphere is stickier the smaller τ is. In the limit τ tends to infinity, the pair potential reduces to a hard sphere potential. By equating the respective second virial coefficients, one can map the square-well potential parameters into an equivalent sticky-sphere potential parameter in the following way: $1/\tau = 12(\Delta/a)\exp(\beta\varepsilon)$, where β is $1/k_B T$. We assume here that $a \gg \Delta$. It is seen from this equation that the stickiness increases as Δ/a or $\beta\varepsilon$ increase. For

an AOT in decane, the parameter Δ corresponds roughly to the length of the hydrocarbon tail, which can stretch out as the temperature increases.

Baxter [12] showed that the Ornstein–Zernike equation for this sticky pair-potential can be solved analytically in the Percus–Yevick approximation [13]. The PY approximation in this case amounts to a reasonable ansatz that the direct correlation function $c(r)=0$ outside the range of the potential a. Combining this ansatz with the exact boundary condition for hard spheres that the pair-correlation function $g(r)=0$ inside the hard core a and has a form of delta function on the surface of the sphere, the direct correlation function inside the hard core can be found. Thus one can obtain an analytical form of the three-dimensional Fourier transform of the direct correlation function $c(k)$ as a function of the volume fraction of the spheres η and the stickiness parameter $1/\tau$. Here $\eta=\rho a^3\pi/6$, and ρ is the number density of the particles. In comparing the theory with experiments for the scattering intensities, we identify η with ϕ.

First, the interparticle structure factor $S(k)$ is calculated from the relation: $S(k)=1/[1-\rho c(k)]$. From the limiting value $S(k\to 0)=\rho k_B T\chi_T$ we can get the isothermal compressibility χ_T. By integrating χ_T with respect to the number density, one obtains the compressibility equation of states. From the equation of state, one finds the existence of a gas–liquid phase transition with a critical point occurring at $\eta_c=0.1213$ and $\tau_c=0.0976$. Again, by integrating the compressibility equation of state, Barboy [14] was able to obtain an analytical chemical potential μ valid in both the one- and the two-phase regions. Having the chemical potential and pressure, one can then obtain the coexistence curve by solving for the coexisting gas and liquid densities at a given τ, which is less than τ_c in the two-phase region.

It is seen that the coexistence curve is highly skewed toward the low-volume fraction side, a feature which is often seen in micellar solutions and microemulsions. This is due to the interaction which is short range and strong and is in sharp contrast to the well-known Van der waal case, which is derived from an interaction that is long range and weak.

One of the nicest feature of Baxter's model is, however, that one can also derive analytically the percolation loci in the $\{\tau,\eta\}$ plane. Coniglio *et al.* [15] introduced a pair-connectedness function $P(r)$ in 1977 in connection with development of a continuum percolation theory. Given a particle at the origin, $4\pi r^2\rho P(r)\,dr$ is the number of particles in the spherical shell $(r, r+dr)$ which are connected to this central particle and belong to the same cluster. Coniglio *et al.* showed that $P(r)$ also satisfied an Ornstein–Zernike-type equation with a modified direct correlation function $c^+(r)$. By invoking the short-range nature of the direct correlation function, namely, $c^+(r)=0$, for $r>a$, and the sticky-sphere condition, $P(r)=(1/12)\,\lambda a\,\delta(r-a)$. Chiew and Glandt [16] were able to show that the

average cluster size S is given by $S = 1/(1-\lambda\eta)^2$. The onset of percolation can be defined as the point where S diverges. Thus the percolation locus in the $\{\tau, \eta\}$ plane is given by $\eta = 1/\lambda$, leading to the equation

$$\frac{1}{\tau} = \frac{12(1-\eta)^2}{19\eta^2 - 2\eta + 1} \tag{1}$$

Figure 1 also shows a percolation line according to Eq. (1).

To compare the theoretical phase diagram with the actual one, we have to specify the relationship between the stickiness parameter $1/\tau$ and the temperature. The simplest relationship with two parameters α and γ is

$$\frac{\tau_c}{\tau} = 1 - \alpha\left(1 - \frac{T}{T_c}\right)^{\gamma} \tag{2}$$

We can try to fit the experimental coexistence curve using the sticky-sphere model supplemented by Eq. (2) and then predict the percolation loci with it. Figure 1 shows the results of choosing $\alpha = 11$ and $\gamma = 0.94$.

3. ANALYSIS OF SANS DATA BELOW T_c

The SANS intensity distribution from a system of polydispersed spherical droplets can be written as [17]

$$I(Q) = (\Delta\rho)^2 \phi_w \left(\frac{4\pi}{3}\bar{R}^3\right) \frac{(Z+6)(Z+5)(Z+4)}{(Z+1)^3} \langle \bar{P}(Q)\rangle \langle S(Q)\rangle \tag{3}$$

where $\Delta\rho = \rho_w - \rho_s$ is the difference of scattering length densities of D_2O and protonated decane, ϕ_w the volume fraction of D_2O, $\bar{R} = \langle R\rangle$, the average radius of the water core, and Z the index related to the polydispersity. The normalized, volume square-averaged particle structure factor is defined as

$$\langle \bar{P}(Q)\rangle = \langle R^6[3j_1(QR)/(QR)]^2\rangle / \langle R^6\rangle \tag{4}$$

The form factor of a spherical particle of radius R is $F(Q) = 3j_1(QR)/(QR)$. The form factor-averaged interparticle structure factor is defined as

$$\langle S(Q)\rangle = \sum_{i,j}^{p} (\rho_i \rho_j)^{1/2} F_i(Q) F_j(Q) S_{ij}(Q) \Big/ \sum_{i}^{p} \rho_i F_i^2(Q) \tag{5}$$

The size average is taken with respect to a Schultz distribution, which is known to be accurate in the case of the AOT/water/decane system [2].

In this case the degree of polydispersity is $\Delta R/\langle R\rangle = (1+Z)^{-1/2}$. The partial structure factor, $S_{ij}(Q)$, for a multicomponent sticky-sphere system has been given by Robertus *et al.* [18], for $i, j = 1$ to 9, using Baxter's method. The FORTRAN package for calculating the partial structure factors has been kindly supplied to us by J. G. H. Joosten. The volume square-averaged particle structure factor, for a Schultz distribution of sizes, had previously been given in an analytical form by Kotlarchyk and Chen [19].

Equation (3) is a theory containing three adjustable parameters $\langle R\rangle$, Z, and τ. These parameters are functions of temperature and volume fraction. Here we assume that particles of different sizes have the same degree of stickiness.

Figure 2 shows results of the analyses of the temperature dependence of the scattering intensity distributions from the 8% (the critical volume fraction) sample. The fits are satisfactory; from them, we were able to extracted three parameters, $\langle R\rangle$, τ, and Z. As temperature increases from 30 to 35 and to 40°C the stickiness parameter progressively decreases toward the critical value, while the average size decreases and the width of the size distribution increases slightly. $Z = 10$, corresponding to a polydispersity index of 30%.

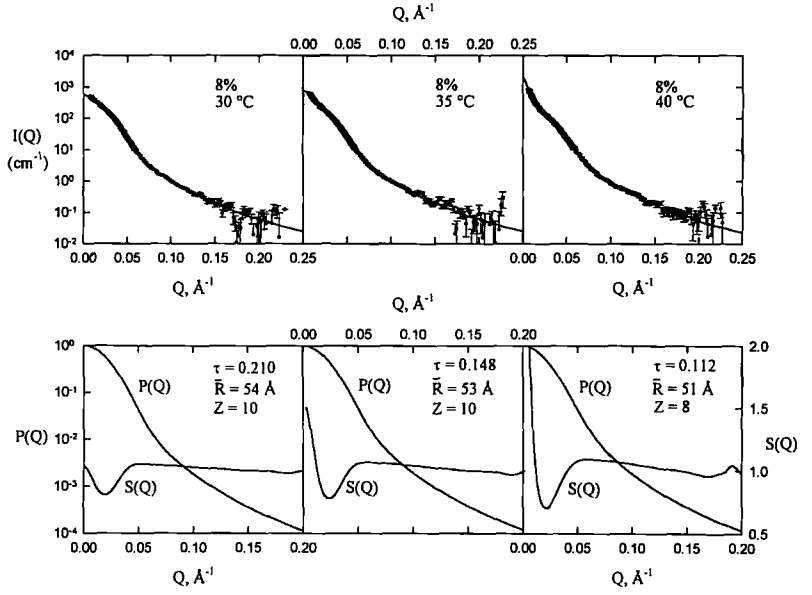

Fig. 2. SANS intensity distributions of the 8% sample as a function of temperature. It is notable that $S(Q)$ increasingly peaks in the forward direction as the temperature approaches the critical point. The particle sizes and size distributions, however, stay the same.

As can be seen, the form factor-averaged interparticle structure factor shows a zero-angle peak due to critical scattering and is devoid of the first diffraction peak due to the low volume fractions.

4. ANALYSIS OF THE PHASE DIAGRAM

It is most reassuring to see that the temperature variation of τ_c/τ derived from SANS data comes out in the form as given in Eq. (2). This situation is similar to the case of nonionic micellar solution investigated by Menon *et al.* [20]. These authors suggested a linear relation between τ_c/τ and T/T_c. Figure 3 plots the τ_c/τ values obtained from SANS data against $(1 - T/T_c)^{0.94}$. Linear relations are obtained by adjusting the value of T_c. For 8% case, the T_c turns out to be 42.7°C, close to the actual T_c in a D_2O-based microemulsion system. The slope of the straight line in Eq. (2) gives $\alpha = 11.03$.

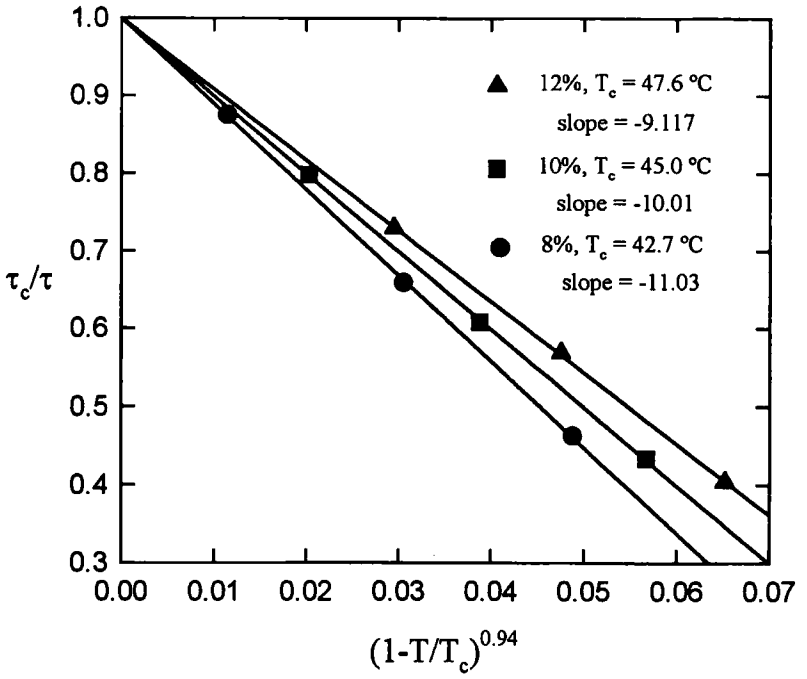

Fig. 3. The stickiness parameter $1/\tau$ extracted from SANS data is plotted as functions of $(1 - T/T_c)^{0.94}$ to obtain the slope $-\alpha$ and T_c. This value of a for 8% volume fraction is used to calculate the theoretical coexistence curve shown in Fig. 1. It is remarkable that the T_c obtained from the 8% data agree with the experimental T_c measured for AOT microemulsion made with D_2O.

We can derive Eq. (2) heuristically in the following way: we study the low-Q behavior of the form factor-averaged structure factor $S(Q)$ for a system of sticky hard spheres of an average diameter 100 Å and a polydispersity index of $Z = 10$ at the critical volume fraction $\eta_c = 0.1213$. The study shows that at sufficiently small Q, the Ornstein–Zernike functional form is obtained and we can thus extract the long-range correlation length ξ as a function of $1/\tau$ as we approach the critical point. If we plot correlation length against $[1-(\tau_c/\tau)]$ on a double-logarithmic scale, we obtain a series of straight lines, implying the validity of a relation

$$\xi \sim \left(1 - \frac{\tau_c}{\tau}\right)^{-\nu'} \tag{6}$$

where the exponent ν' depends on the polydispersity index Z. When Z is very large, namely, when the system consists of monodisperse sticky-spheres, $\nu' = 0.5$; but when $Z = 10$, corresponding to the system under study, $\nu' = 0.532$. On the other hand, it is known experimentally as well as theoretically that near the critical point of a fluid, the correlation length is a function of the temperature distance from the critical point according to

$$\xi \sim \left(1 - \frac{T}{T_c}\right)^{-\nu} \tag{7}$$

with $\nu = 0.5$, as in a mean field theory, such as in Baxter's solution. Equations (6) and (7) taken together lead to our previous ansatz, Eq. (2), in which $\gamma = \nu/\nu' = 0.500/0.532 = 0.94$.

Figure 1 shows a comparison of the experimental cloud point curve (open circles) and the theoretical coexistence curve (solid line) and spinodal line (dashed line) calculated by the polydisperse sticky-sphere model, with the stickiness parameter τ depending on temperature according to a relation

$$\frac{\tau_c}{\tau} = 1 - 11\left(1 - \frac{T}{T_c}\right)^{0.94} \tag{8}$$

To account completely for the percolation locus from Eqs. (1) and (2), we have to introduce a temperature-dependent effective sticky-sphere diameter. This idea is a reasonable one because the definition of connectivity of two spheres should be dependent on the thermodynamic state of the liquid. In fact it is intuitively appealing to postulate that the higher the temperature, the easier it is for the counterions to migrate from one water core of a droplet to another in the neighborhood. Therefore the effective diameter of the microemulsion droplets, as far as electrical percolation is

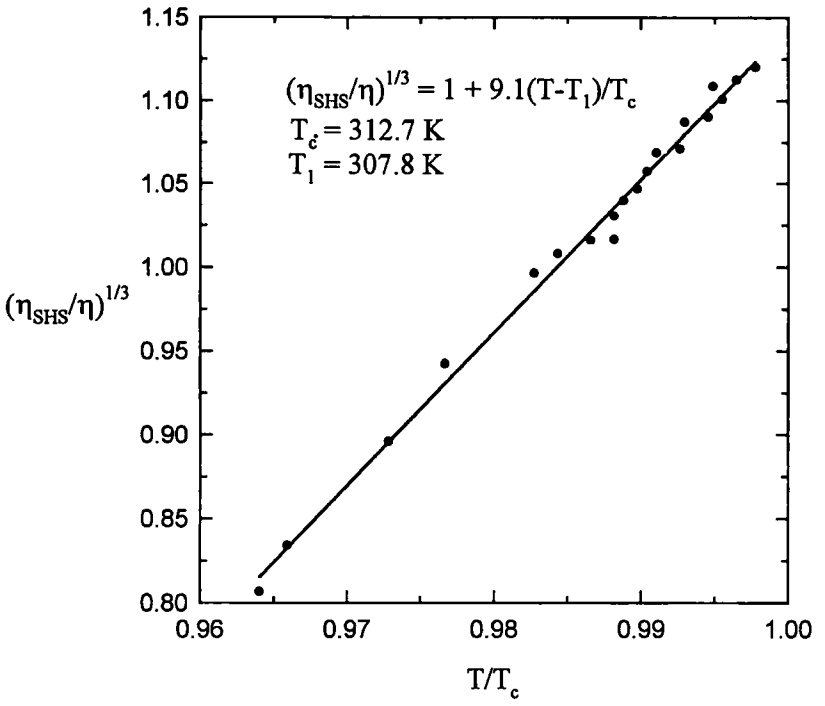

Fig. 4. The temperature dependence of the apparent volume fraction η_{SHS} of sticky spheres which are needed to fit the percolation line. We plot the ratio $(\eta_{SHS}/\eta)^{1/3}$ versus T/T_c, which results in a straight line. This shows that the apparent diameter of sticky spheres which is percolating increases linearly as the temperature increases.

concerned, is larger for higher temperatures. Figure 4 shows the result of force-fitting the experimental percolation locus (filled circles) with Eq. (1) (solid line). The ratio, $(\eta_{SHS}/\eta)^{1/3}$, which is a measure of the ratio of the effective diameter to the actual diameter, turns out to be a linear function of T/T_c. It is shown in Fig. 4 as a solid line.

5. DYNAMICS OF THE DROPLET NUMBER DENSITY FLUCTUATION NEAR THE CRITICAL POINT

We turn next to the discussion of some aspects of the droplet dynamics near the critical point. The starting point of our theory is the assumption that the slow dynamics of the droplets is dominated by diffusive motions of the percolation clusters [21]. This assumption is expected to be good in the vicinity of the percolation threshold, where large, transient fractal clusters are formed. Formation of the transient fractal clusters is a necessary condition

for the dynamic percolation theory [9] to be valid. We have used it to explain the conductivity exponent below the percolation threshold in the introduction. In the AOT/water/decane system, as one can see from the phase diagram (Fig. 1), the critical point is only about 2° above the percolation point. One therefore expects that the cluster structure and cluster size distribution in the critical region are similar to the percolation point.

For light scattering, the wavelength of visible light is much larger than the droplet sizes. Hence, for this Q range, the particle structure factor is nearly unity and we can ignore it.

First, the interparticle structure factor $S_k(Q)$ for a cluster containing k particles in given by [22]

$$S_k(Q) = \frac{k\,D\Gamma(D)\sin[(D-1)\tan^{-1}(QR_k)]}{(D-1)\,QR_k[1+Q^2R_k^2]^{(D-1)/2}} + 1 \tag{9}$$

where D is the fractal dimension of the clusters, $R_k = R_1 k^{1/D}$, the radius of gyration of the k-cluster, and R_1 the average radius of the droplet. The intermediate scattering function $F(Q, t)$ can then be calculated as

$$F(Q, t) = \frac{\sum_{k=1}^{\infty} kN(k)\,S_k(Q)\exp(-D_k Q^2 t)}{\sum_{k=1}^{\infty} kN(k)\,S_k(Q)} \tag{10}$$

The discrete sum can be converted into an integral over k by introducing a cluster size distribution function of the form $N(k) \approx k^{1-\tau}\exp(-k/S)$ [23]. In this expression τ is the polydispersity exponent, S the average cluster size, $D_k = D_1 k^{-1/D}$ the translational diffusion coefficient of the k-cluster, and D_1 the Stokes–Einstein diffusion coefficient of the droplet. Numerical simulations for three-dimensional percolation clusters gave a fractal dimension $D = 2.5$ and the polydispersity exponent $\tau = 2.2$ [23]. The measured photon correlation function is then given by $C^2(Q, t) = 1 + |F(Q, t)|^2$. The first cumulant, or the average relaxation rate $\Gamma(Q)$, is the logarithmic derivative of $C(Q, t)$ evaluated at $t = 0$.

5.1. Dynamic Slowing-Down of the Average Relaxation Rate

The average relaxation rate $\Gamma(Q)$ can be expressed in terms of two dimensionless variables, $x = Q\xi$ and $x_1 = QR_1$, where the correlation length is defined as $\xi = R_1 S^{1/D}/[3]^{1/2}$. The complete analytical form of the $\Gamma(Q)$ near the percolation threshold has been given in Ref. 21. We limit our discussion here to the particular case near the critical point. In this case the cluster structure factor Eq. (9) is approximated by its low-Q form $S_k(Q) = k\exp(-Q^2R_k^2/3)$. An analytical expression of $\Gamma(Q)$ can be obtained by an

integration. It is more revealing to display a scaling function defined as $\Gamma^*(x, x_1) = \Gamma(Q)/D_1 R_1 Q^3$. It is [24]

$$\Gamma^*(x, x_1) = \frac{3\pi}{8} \frac{\Gamma(3-\tau, x_1^D)\,\Gamma(3-\tau-1/D, u)}{\Gamma(3-\tau-1/D, x_1^D)\,\Gamma(3-\tau, u)} \left[1+\frac{1}{x^2}\right]^{1/2} \tag{11}$$

where $u = (x_1/x)^D [1+x^2]^{D/2}$, and $\Gamma(a, b)$ is the incomplete Euler gamma function. It should be remarked that the presence of the second nonuniversal variable x_1 in Eq. (11) is due to the finite size of the constituent particles. It is remarkable that in the limit of small particles, $\Gamma^*(x, x_1)$ reduces to the Kawasaki universal dynamic scaling function calculated by a mode coupling theory, which is known to account for light-scattering data from binary mixtures of molecular liquids very well. $\Gamma^*(x, x_1 = 0)$ has simple asymptotic behavior: For $x \ll 1$, $\Gamma^*(x) = a/x$, and for $x \gg 1$, $\Gamma^*(x) = b$, where a and b are known constants. Figure 5 illustrates the crossover from small x to large x behavior as given above. Using light-scattering data taken near the critical point of the AOT/water/decane system, we illustrate the agreement of measured first cumulants of photon correlation functions and prediction of Eq. (11) [24]. It is clear from the graph that the finite size effect of microemulsion droplets is large enough to be detectable in a light-scattering experiment.

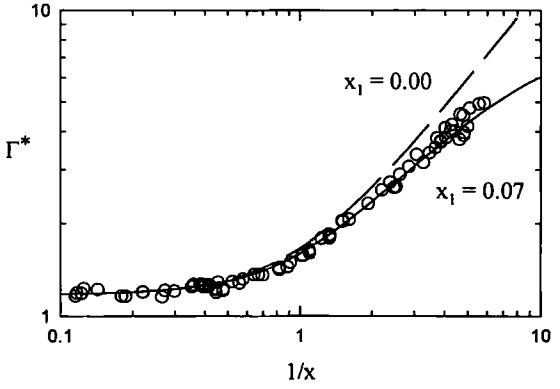

Fig. 5. The dynamic scaling function $\Gamma^*(x, x_1)$ associated with the first cumulant of the photon correlation function plotted as a function of $1/x$ for two values of the scaled droplet size x_1. Open circles are experimental data from the AOT/water/decane system near the critical point. The upper solid line corresponds to Kawasaki's mode–mode coupling result. The lower solid line is the dynamic droplet-model result presented in the text.

An analogous dynamic slowing-down phenomenon near percolation points at higher volume fractions has been observed and explained by the theory [21, 25].

5.2. Stretched Exponential Decay of the Time Correlation Function at Long Times

Again Eq. (10) in its integral form can be computed analytically [26]. We then obtain the time correlation function, $C(u, v)$, in terms of the scaling variable u and a dimensionless time variable $v = D_1 R_1 Q^3 t(1 + x^{-2})^{1/2}$. It is sufficient for the purpose here to state that at sufficiently short times, we have an exponential decay with the average relaxation rate $\Gamma(Q)$ given before, $C(u, v \to 0) = \exp[-\Gamma(Q)\, t]$. At long times such that $\Gamma t \gg 1$, the time correlation function approaches an stretched exponential form, $C(u, v \gg 1) = \exp[-(\bar{\Gamma} t)^{\beta}]$, with $\bar{\Gamma}$ given by

$$\bar{\Gamma} = \beta^{1/\beta} D^{1/D} D_1 R_1 q^3 \left(1 + \frac{1}{x^2}\right)^{1/2} \tag{12}$$

and the exponent $\beta = D/(D+1)$ is a universal number 0.713.

Crossover from the short-time exponential decay to the long-time stretched exponential decay of the photon correlation function occurs at the dimensionless variable $\Gamma t = 1$.

Near the percolation points at high volume fractions, one has a similar crossover from exponential to stretched exponential behavior [21], except the crossover occurs at earlier times so the stretched exponential decays can be easily observed in experiments [17].

6. CONCLUSION

We have given concrete evidence that both the structure and the dynamics observed in a three-component microemulsion system, AOT/water/decane, near the critical and percolation points can be explained in terms of a model based on the formation of transient, polydisperse fractal clusters due to a short-range attraction between microemulsion droplets. This attractive interaction increases in a specific way as the temperature increases toward the percolation and critical points. We derive a quantitative relation between the interaction strength and the temperature from analyses of SANS data in the one-phase region approaching the critical point. This relation serves to explain the overall feature of the phase diagram, including the cloud point curve and the percolation line.

The diffusive cluster dynamics also accounts for the Q dependence of the first cumulant of photon correlation functions in the critical region. The dynamic scaling function associated with the average relaxation rate deviates significantly from the well-known Kawasaki function at large Q due to the large sizes of the microemulsion droplets [24]. The long-time behavior of the photon correlation function is shown to be a stretched exponential form with a universal stretch exponent of 0.713 [21].

ACKNOWLEDGMENTS

The research of S. H. Chen and C. Y. Ku is supported by a grant from the Material Science Division of the U.S. Department of Energy and The Center for Materials Science and Engineering of MIT. We are grateful for the use of the NSF 30-m CHRNS spectrometer at the Cold Neutron Research Facility of the National Institute of Standard and Technology, where these SANS measurements were carried out.

REFERENCES

1. S. H. Chen, S. L. Chang, and R. Strey, *J. Chem. Phys.* **93**:1907 (1990).
2. M. Kotlarchyk, S. H. Chen, J. S., Huang, and M. W. Kim, *Phys Rev.* **A29**:2054 (1984).
3. M. Kotlarchyk, S. H. Chen, J. S. Huang, and M. W. Kim, *Phys Rev. Lett.* **53**:914 (1984).
4. L. Auvray, J. P. Cotton, R. Ober, and C. Taupin, *J. Phys. Chem.* **88**:4586 (1984).
5. F. Lichterfeld, T. Schumeling, and R. Strey, *J. Phys. Chem.* **90**:5762 (1986).
6. S. H. Chen, S. L. Chang, R. Strey, J. Samseth, and K. Mortensen, *J. Phys. Chem.* **95**:7427 (1991).
7. J. Rouch, A. Safouane, P. Tartaglia, and S. H. Chen, *J. Chem. Phys.* **90**:3756 (1990).
8. C. Cametti, P. Codastefano, P. Tartaglia, J. Rouch, and S. H. Chen, *Phys. Rev. Lett.* **64**:1461 (1990).
9. G. S. Grest, I. Webman, S. Safran, and A. L. R. Bug, *Phys. Rev.* **A33**:2842 (1986).
10. M. Lagues, *J. Phys. (Paris) Lett.* **40**:L331 (1979).
11. J. P. Clerc, G. Giraud, J. M. Laugier, and J. M. Luck, *Adv. Phys.* **39**:191 (1990).
12. R. J. Baxter, *J. Chem. Phys.* **49**:2770 (1968).
13. J. K. Percus and G. J. Yevick, *Phys. Rev.* **110**:1 (1958).
14. B. Barboy, *J. Chem. Phys.* **61**:3194 (1974).
15. A. Coniglio, U. De Angelis, and A. Forlani, *J. Phys.* **A10**:1123 (1977).
16. Y. C. Chiew and E. D. Glandt, *J. Phys.* **A16**:2599 (1983).
17. E. Y. Sheu, S. H. Chen, J. S. Huang, and Y. C. Sung, *Phys. Rev.* **A39**:5867 (1989).
18. C. Robertus, W. H. Philipse, J. G. H. Joosten, and Y. K. Levine, *J. Chem. Phys.* **90**:4482 (1989)
19. M. Kotlarchyk and S. H. Chen, *J. Chem. Phys.* **79**:2461 (1983).
20. S. V. G. Menon, V. K. Kelker, and C. Manohar, *Phys. Rev.* **A43**:1130 (1990).
21. P. Tartaglia, J. Rouch, and S. H. Chen, *Phys. Rev.* **A45**:7257 (1992).
22. S. H. Chen and J. Teixeira, *Phys. Rev. Lett.* **57**:2583 (1986).

23. D. Stauffer, *Phys. Rep.* **54**:1 (1979).
24. J. Rouch, P. Tartaglia, and S. H. Chen, *Phys. Rev. Lett.* **71**:1947 (1993).
25. S. H. Chen, F. Mallamace, J. Rouch, and P. Tartaglia, in *Slow Dynamics in Condensed Matter*, K. Kawasaki, T. Kawakatsu, and M. Tokuyama, eds. (American Institute of Physics, New York, 1992.), p. 301.
26. S. H. Chen, J. Rouch, and P. Tartaglia, *Croatica Chem. Acta* **65**:353 (1992).